The Effect of Hydroxyl Spacing in Diols on the Solvation Structure, Dynamics, and Transport Properties of Choline Chloride-Based Deep Eutectic Solvents

Rathiesh Pandian[1], Daniel Kim[2], Yong Zhang[2], Sunjuezhe Wang[1], Giselle de Araujo Lima e Souza[3], Steven Greenbaum[3*], Edward Maginn[2*], Clemens Burda[1*]

[1]Department of Chemistry, College of Arts and Sciences, Case Western Reserve University, Cleveland, OH 44106, USA

[2]Department of Chemical and Biomolecular Engineering, College of Engineering, University of Notre Dame, Notre Dame, IN 46556, USA

[3]Department of Physics & Astronomy, Hunter College of the City University of New York, New York, NY 10065, USA

* Corresponding author. E-mail address: Burda@case.edu (C. Burda)

Abstract

Deep eutectic solvents (DESs) are a class of liquids that offer great potential in alleviating some of the challenges present in today's long-term energy storage methods because they have physical properties that are favorable for storable electrolyte solutions. In this work, a series of glycols (ethylene glycol, 1,3-propanediol, 1,4-butanediol, and 1,5-pentanediol) were studied as potential hydrogen bond donors (HBD) with a common choline chloride (ChCl) as the hydrogen bond acceptor (HBA). The solvation dynamics of the prepared systems were studied by measuring the solvent reorganization response using femtosecond transient absorption spectroscopy (fs-TA). Conductivity, viscosity, density, $E_T(30)$ polarity, and dynamics of the prepared DESs were analyzed, with a particular interest in determining the effect of HBD chain length on these parameters. Classical molecular dynamics simulations were employed to investigate how the local liquid structure, solvent dynamics, and bulk solvent properties vary with changes in glycol chain length.

1. Introduction

Deep eutectic solvents (DESs) have emerged as a promising type of liquid resulting from the combination of a hydrogen-bond donor (HBD) and a hydrogen-bond acceptor (HBA) in a specific ratio. Their discovery by Abbott et al. in 2003 stemmed from the observation that adding choline chloride (ChCl) to urea resulted in a reduced melting point, which could be lowered until reaching the eutectic composition.[1,2] This unique class of solvents has garnered significant attention in recent years due to their desirable attributes. Many DES exhibit excellent thermal and chemical stability, low volatility and flammability, low toxicity, biodegradability, and cost-effectiveness. These properties, largely attributed to hydrogen-bonding interactions,[3–8] have led to their investigation as electrolytes in batteries and fuel cells.[2,4,5]

When coupled with renewable energy sources, redox flow batteries (RFBs) offer a valuable means of storing excess energy for future use. Due to their environmental compatibility, high storage capacity, and high responsiveness, they may be beneficial for long-term storage batteries, helping to limit environmental pollution.[9–11] In the last 20 years, numerous DES systems have

been studied for such energy applications. One of the most studied DESs consists of a 1:2 molar ratio of ChCl (33.33 mol % ChCl) and the diol ethylene glycol (EG), often referred to as "ethaline."[5] Due to the strong intermolecular hydrogen bond network present within pure EG, as well as the *gauche* conformation being most stable, EG molecules have been reported to chelate.[12–17] The addition of ChCl induces a perturbation in the hydrogen bond network of EG, leading to the occasional formation of bidentate hydrogen bonds between the hydroxyl groups of EG and Cl^- anions. The intricate hydrogen-bond architecture within DESs exerts a profound influence on their physical and chemical attributes, comprising but not limited to viscosity, melting point, density, dynamics, and charge transport phenomena.[15,18–20]

The hydrogen-bonding interactions present in ethaline have been investigated via extensive computational work. Zhang et al.[18] quantified the various hydrogen-bonding interactions present in ethaline to find that HBs between the Cl and EG hydroxyl groups are stronger than HBs between the hydroxyl groups of two EG molecules. Alizadeh et al. [21] examined the composition effect on the structure and conformation of EG using 1:1 and 1:2 mixtures of ChCl:EG and found that the gauche-to-trans conformer ratio of EG in the 1:1 ratio is almost double that of the 1:2 ratio mixture. Gaur et al[22] reported the significance of intramolecular hydrogen bonding present in EG in the consideration of overall EG-EG hydrogen-bond interactions, in addition to the typical intermolecular HBs considered. Despite numerous studies published on ChCl:EG systems, the complexities of hydrogen-bond networks motivate further research into how chemical and structural features can lead to different solvent properties in other DES systems.

The exploration of diols as HBDs in DESs has expanded beyond EG to encompass propanediols, butanediols, and pentanediols in recent years.[23–28] The elongation of the carbon chain relative to EG enables a more in-depth investigation of the intricate hydrogen-bond network present in DESs, as well as its consequential impact on their properties. With increasing alkyl chain length and hydroxyl separation, intramolecular hydrogen bonding appears to become more robust in pure diols. For instance, in 1,4-butanediol, hydrogen bonding can give rise to both linear and cyclic aggregates.[29,30] However, Chen et al. have revealed that 1,5-pentanediol demonstrates weaker intramolecular hydrogen bonding than 1,4-butanediol.[31] This could be attributed to the fact that the hydroxyl groups in 1,5-pentanediol are located at the molecule's extremities, leading to the formation of layer-like structures through hydrogen bond-induced self-

association.[32] In addition, Cerar et al have discovered that the longer the alkyl chain of the diols, the more inclined they are to adopt a more stretched molecular conformation.[17] In summary, while cyclic aggregates are conceivable, pure diols are more inclined to exist as linear structures as the alkyl chain length increases.

In addition to ethaline, other DES systems have been explored. Urea-based DESs tend to have decent suppression of melting point, with the lowest melting point being 12 °C at its eutectic composition of 33.33 mol % ChCl (referred to as "reline"). However, even at the eutectic composition, its viscosity is high (~1000 mPa s) and conductivity is low (~1 mS cm^{-1}), making their potential use as electrolytes for RFBs quite limited.[2] ChCl + glycerol mixtures, referred to as "glyceline" at its eutectic composition of 33.33 mol % ChCl, have also received significant attention. Unfortunately, being a triol, the glycerol-based DESs suffer from high viscosities and low conductivities, limiting their usability for battery electrolyte applications.[33,34] When tuning the halide (F^-, Cl^-, Br^-, I^-) bound to choline in DESs with EG, chloride offered the most optimized conductivity and viscosity, along with the fastest dynamics.[35] Thus, an ideal DES for desired energy applications should consist of ChCl mixed with a diol like EG.

Recently, we have explored other diol systems to study the effects of alkyl chain length and hydroxyl group spacing in a small series of diols. ChCl was mixed with either 1,2-propanediol or 1,3-propanediol at varying compositions and compared to ChCl:EG mixtures.[36] To expand on these comparisons, we now investigate a broader series of diol-based DESs to assess how variations in hydroxyl spacing influence their physical properties and solvation dynamics. In this work, we explore the properties of four diol-based DESs formed by mixing ChCl with EG (1,2-Eth), 1,3-propanediol (1,3-Pro), 1,4-butanediol (1,4-But), or 1,5-pentanediol (1,5-Pen), to investigate how the spacing of carbon atoms between terminal hydroxyl groups affects their viscosity, conductivity, density, as well as solvent polarity and solvation dynamics. See Scheme 1 for molecular structures of compounds studied in this work.

To date, there has been limited literature on these novel systems, especially on properties such as polarity and dynamics. Dynamical studies were based on the solvent relaxation response to a reporter molecule, Reichardt's dye betaine 30 (B30), which undergoes an ultrafast intramolecular charge transfer (CT) process upon photoexcitation. This CT process results in a significant change in dipole moment (~21 Debye),[37] with the excited state being less polar than

the ground state, causing the surrounding solvent molecules to adjust their orientation to accommodate the change, as shown in Scheme 1.[38–43] Multiple studies conducted by different research groups have demonstrated that the rate-limiting factor for the measured back electron transfer kinetics is the solvent's reorganization response rather than the probe molecule. This means that the intramolecular CT process is considered instantaneous in comparison to solvent reorientation.[44,45] In complex mixtures such as DESs, choline is the solvation component that is primarily the most rate-limiting.[41] In this study, we utilized the B30 probe to investigate the solvent relaxation dynamics in various DES systems, which have been minimally studied in this regard to date.[45–49] In addition to examining dynamics, we also utilized the B30 probe to measure solvent polarity. To achieve this, we employed UV-vis spectroscopy to measure the absorption of DESs containing B30 and utilized the $E_T(30)$ scale as a tool to determine polarity.[39,41,48,50–52] The studied systems were also simulated using classical molecular dynamics. Simulations were validated against experimental measurements and further analyzed to explore the local liquid structure, as well as components of the solvent dynamics. We present a comprehensive outline of the molecular-level differences between diol systems and how these differences translate to bulk-scale properties important for electrolyte applications, also highlighting both differences and similarities between the well-established 1,2-Eth, or ethaline, DES and longer diol systems. From key bulk properties, such as density, conductivity, and viscosity, to in-depth solvent characteristics, including polarity, relaxation dynamics, self-diffusion coefficients, coordination numbers, residence times, and static dielectric constants, structure-property relationships are explored to leverage these insights for designing high-performance electrolytes.

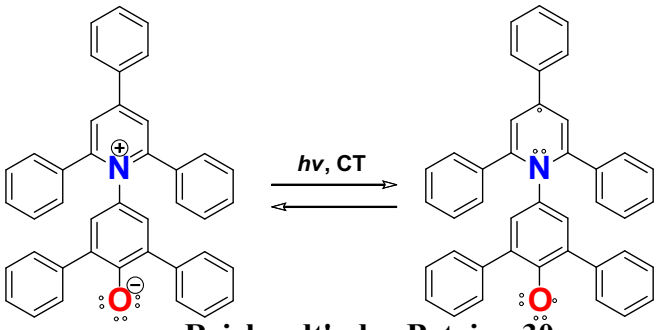

Reichardt's dye Betaine-30 (B30)

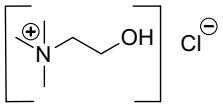

Choline chloride (ChCl)

+

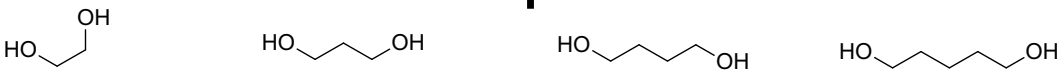

Ethylene glycol (1,2-Eth) | **1,3-Propanediol (1,3-Pro)** | **1,4-Butanediol (1,4-But)** | **1,5-Pentanediol (1,5-Pen)**

Scheme 1. Representative molecular structures illustrating the laser-induced intramolecular charge transfer process in B30, transitioning from its zwitterionic ground state to its radical excited state (shown left to right). The molecular structures of ChCl, ethylene glycol (EG), 1,3-propanediol, 1,4-butanediol, and 1,5-pentanediol are also shown. ChCl mixed with EG, 1,3-propanediol, 1,4-butanediol, or 1,5-pentanediol are called 1,2-Eth, 1,3-Pro, 1,4-But, or 1,5-Pen, respectively.

2. Experimental

2.1. Experimental Methods:

2.1.1. Materials

Choline chloride (ChCl) (≥98%), 1,4-butanediol (ReagentPlus®, 99%), 1,5-pentanediol (≥97.0%), and Reichardt's dye (B30) (90%) were purchased from Sigma-Aldrich. 1,3-propanediol (98%) and ethylene glycol (≥99%) were purchased from Acros Organics.

2.1.2. Preparation of binary mixtures

Before preparing the binary mixtures, the ChCl underwent vacuum and heat drying for 72 hours, followed by storage in an argon-filled glove box to ensure an ultra-dry environment. The diol solvents were similarly dehydrated using molecular sieves. In the glove box, the ChCl was accurately weighed, immediately capped, and ultimately sealed to prevent water absorption. A predetermined quantity of the dried diol was swiftly added to the ChCl to create a stock solution, which was then sonicated and heated until a homogeneous and transparent solution was achieved. Dilutions were subsequently performed to achieve the targeted molar ratios. Due to the limitations in maintaining liquid samples at our ambient lab temperature, ChCl compositions exceeding 30 mol % for 1,3-Pro and 20 mol % for 1,4-But and 1,5-Pen could not be explored. All measurements were performed immediately after sample preparation to minimize the influence of water uptake since these mixtures are highly hygroscopic.

2.1.3. Measurements of Viscosity and Density

At a temperature of 298 K, the viscosity (η) of the mixtures was evaluated by introducing around 100 μL of the sample into a Rheosense microVISC viscometer. The measurements were performed in triplicate and the results were averaged, with standard deviations provided. Additionally, the density (ρ) of the samples was determined by using an Anton Paar DMA-5000 density meter, in which the measurements were carried out at temperature intervals of 5 K, ranging from 298 to 323 K, with a standard deviation of $\leq$ 0.20 K. The calibration of the density meter was conducted with degassed deionized water, where the maximum density deviation was determined to be 5×10^{-5} g mL^{-1} at 293 K.

2.1.4. Measurements of Ionic Conductivity

A Thermo Scientific Orion Star A222 conductivity meter with a 2-electrode conductivity cell, with a measurement range of 10 to 2000 mS cm^{-1}, was employed to determine the ionic conductivity (σ) of the samples at 298 K. Three standard sodium chloride solutions with conductivities of 0.100, 1.413, and 12.9 mS cm^{-1} were used to calibrate the instrument. Triplicate

measurements were performed on each sample, and the results were averaged to obtain an overall value, with standard deviations shown in the data.

2.1.5. *Measurements of Solvent Polarity and Relaxation Kinetics*

A Varian Cary 50 UV-Vis spectrophotometer was used to measure steady-state absorption spectra. To obtain an optical density of 0.5 per 0.2-centimeter optical pathlength, a small amount of Reichardt's dye (B30) was added to each solution. The maximum of the absorption band (λ_{max}) was solvatochromic and highly solvent-dependent. The $E_T(30)$ scale, developed by Reichardt, was used to determine the solvent polarity.[39,53] B30 was also utilized to investigate solvent response and kinetics using femtosecond transient absorption (fs-TA) spectroscopy. The use of B30 to better understand solvatochromism and solvation dynamics in various solvent systems was extensively explored by prominent researchers Maroncelli and Barbara in the 1990s.[45,47]

To perform fs-TA spectroscopy measurements, we used a Clark MXR CPA-2010 laser system with a 780 nm fundamental beam that was split into two pathways by a beam splitter. One pathway formed the pump beam, which photoexcited the sample. The beam was generated via frequency doubling of the fundamental beam by a β-barium borate crystal to a wavelength of 390 nm. The other pathway was the probe beam, which was used to measure differential absorption spectra of the sample as a function of delay time. To generate the probe, the fundamental beam was directed towards a sapphire crystal, resulting in a white supercontinuum beam. A computer-controlled optical delay stage was used to create a temporal delay. Steady-state and fs-TA measurements were performed using a 2 mm glass cuvette at ambient lab conditions. Steady-state absorption spectra were taken before and after fs-TA experiments and compared to ensure that no photodegradation of B30 or formation of photoproducts occurred. Chirp correction was performed using Surface Xplorer software, and Microcal Origin Software was employed to conduct the analysis and perform biexponential fitting.

2.1.6. *Pulsed-Field Gradient NMR*

Pulsed-field Gradient NMR analyses were performed on samples placed in 5 mm NMR tubes under an argon glovebox and flame-sealed to prevent exposure to air and moisture. Measurements were conducted at 298.2 K after allowing 15 minutes for thermal equilibration.

Experiments were carried out on a Bruker Avance 400 NMR spectrometer operating at a magnetic field strength of 9.4 T, equipped with a direct observe 5 mm pulsed-field z-gradient BBFO iProbe. Pulsed-field gradient NMR measurements were performed in the ^{1}H domain using the bipolar pulse longitudinal eddy current delay (BPP-LED) pulse sequence. Each experiment consisted of 8 transients per increment, using 16384 points in the F2 dimension and a spectral width of 14 ppm. The relaxation delay was set to at least five times T_1, and four dummy scans were used before acquisition. Gradient strengths were incremented linearly from 2% to 95% of the maximum value (50 $G \cdot cm^{-1}$) over 16 steps. For each experiment, the gradient pulse duration (δ) was optimized within the 4.2–6 ms range, and the diffusion time (Δ) was adjusted between 0.2 and 0.4 s to achieve approximately 95% signal attenuation for the slowest-diffusing species at the final gradient step. The raw spectra were subjected to manual phasing and automatic baseline correction. Data were processed using an exponential filter in the F2 dimension (line broadening = 0.3 Hz). Signal integrals were fitted to the Stejskal–Tanner equation,[54] shown in Equation (1), using the T_1/T_2 module in Bruker TopSpin:

$$\frac{I}{I_0} = e^{\left[-D\gamma^2 g^2 \delta^2 \left(\Delta - \frac{\delta}{3}\right)\right]} \quad (1)$$

where I is the signal intensity with the gradient applied, I_0 is the initial signal intensity, γ is the gyromagnetic ratio of the investigated nucleus, and g is the gradient strength applied.

2.2. Computational Methods

Classical molecular dynamics simulations of the systems were performed using the LAMMPS package (February 7th, 2024 release).[55] The refined general Amber force field (GAFF)[56] was used to describe atomic interactions. EG, ChCl, and 1,3-propanediol force field parameters used are identical to those used in the previous study,[36] and the same optimization procedure outlined in previous work was used to develop force fields for 1,4-butanediol and 1,5-pentanediol interactions. Values for the optimized force field parameters are provided in Table S1 in the Supporting Information (SI). Long-range electrostatic interactions were calculated using the particle-particle particle-mesh (PPPM) method[57] with a real space cutoff of 12 Å. Tail corrections were applied to the van der Waals interactions with a 12 Å cutoff. The initial

configurations for the simulations were generated using the package Packmol[58,59] with different sets of compositions as shown in Tables S2-S4. Each system was equilibrated in the isothermal-isobaric (NPT) ensemble for four ns, and the simulation was then run for an additional 20 ns in the canonical ensemble (NVT) for the production run. The Nosé-Hoover thermostat[60] and extended Lagrangian approach[61] were used to control the temperature and pressure, both with time constants of 100 fs. The pressure was set to 1 atm in the NPT simulations with isotropic volume fluctuations. Periodic boundary conditions were applied in all directions, and a time step of 1 fs was used in all simulations. An example LAMMPS input file is provided in the SI. Methods used to calculate various properties are described in the results section.

3. Results and Discussion

3.1. Density

The experimentally measured densities for all systems as a function of mol % ChCl at room temperature (T = 298 K) and across all measured temperatures are shown in **Figures 1** and S1a, respectively. For all systems, the density increases with increasing ChCl salt concentration, although the increase is minimal for 1,2-Eth, as seen in Figure S1b. Across all systems and salt concentrations, at a given temperature, densities follow the trend of 1,2-Eth > 1,3-Pro > 1,4-But > 1,5-Pen; this shows that density decreases with increasing chain length and O-H spacing. Figure S2 shows the densities of each system as a function of increasing temperature. In all systems, density decreases with increasing temperature. Densities were also obtained from simulations. The uncertainty estimation was carried out using the block averaging method applied to the latter half of the NPT simulation. Calculated densities (Figure 1) show excellent agreement with the experimental values, with a difference of less than 1% for all four systems across all compositions. Simulations perfectly match the order of experimental densities 1,2-Eth > 1,3-Pro > 1,4-But > 1,5-Pen.

The density change upon ChCl addition (the slope in Figure 1) is different for each diol mixture due to the various densities of the pure alcohols. For each diol, the experimental density as a function of ChCl fraction was fit to a linear function and extrapolated to a hypothetical “liquid” ChCl (i.e., pure ChCl is a solid at these temperatures). As shown in Figure 1b, the densities of the

1,3-Pro, 1,4-But, and 1,5-Pen systems converge to a similar "liquid" ChCl density (with the most significant deviation being 0.013 g/cm^3). In contrast, the 1,2-Eth mixtures converged to a slightly lower value. This suggests a different solvation structure in 1,2-Eth than in longer-chain diol DESs, and that the interactions between ChCl and EG are relatively weaker compared to the interactions between ChCl and the other glycols. Calculated densities from simulations show a similar trend, and the fitting results are shown in Figure S3 in the SI.

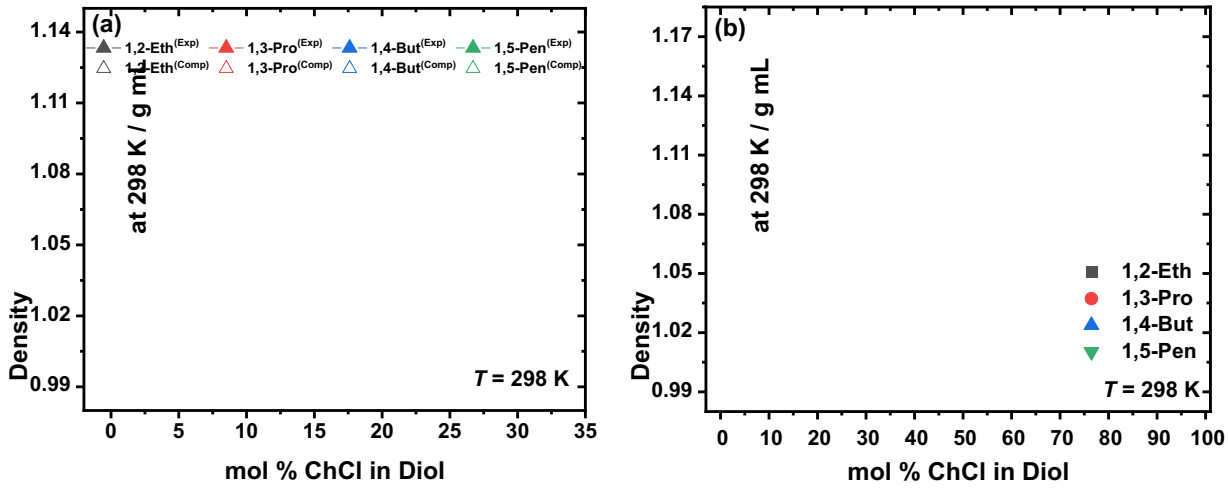

Figure 1. (a) Densities for all systems investigated in this work at room temperature (T = 298 K) as a function of mol % ChCl. Experimental results are shown in solid triangles, and open triangles denote simulation values. See Tables S5-8 for numerical values. Also see Figure S1 for densities of all systems across the 298 – 318 K temperature range. **(b)** Linear fit to the experimental densities of DES systems based on measurements at 298 K and the extrapolation to a hypothetical "liquid" ChCl. The density values are from our previous work.[36]

3.2. Coordination Number and Denticity

Before discussing coordination numbers, we briefly assessed molecular conformations sampled in the simulations to determine whether dihedral preferences vary with diol identity or composition. To address this, dihedral-angle distributions were examined for choline and ethylene glycol at representative compositions. The N–C–C–O dihedral of choline favors a gauche conformation over trans at approximately a 2:1 ratio, while the C–C–O–H dihedral is predominantly anti, resulting in a compact choline structure rather than a fully extended geometry. For ethylene glycol, only gauche O–C–C–O conformations were observed across all compositions. These trends show minimal dependence on composition and are consistent with prior reports that

EG conformation is largely composition-insensitive. Full dihedral distributions are provided in the SI (Figure **S4**).

Given the different mixing behavior of 1,2-Eth compared to the other glycols, the liquid structure was examined via coordination numbers (CNs), as they provide insight into the molecular interactions present in the solutions. Mathematically, CNs are the integrals of the radial distribution functions; they indicate how many molecules or atoms of a particular species are located within the specified coordination sphere around a reference particle. For this study, only interactions within the first solvation shell were quantified to probe the local liquid structure of the solvents, and the first solvation shell cutoff was defined as the first minimum between the first two maxima in the radial distribution function of any interaction considered. Consistent with previous work,[36] two key interactions were chosen for their dominance in solvation: the HO-Cl interaction, representing the H-bond between diol hydroxyl hydrogens and chloride ions (O-H···Cl^-), and the HO-OH interaction, which means the hydrogen bonds between diol molecules (O-H···H-O). **Figure 2** shows the HO-OH CNs in the first solvation shell to be about 1.0 in the pure diols, which decreases with increasing ChCl composition. The HO-Cl CNs, which represent the average number of chloride ions around a diol hydroxyl hydrogen, increase as more ChCl is added to the system, showing the opposite trend of the diol-diol interactions. This overall trend of increasing HO-Cl CNs and decreasing HO-OH CNs is consistent with previous results[55] given the preference of diol molecules to bond with chloride ions over other diol molecules and the increasing number of ChCl molecules present within the system. Surprisingly, no significant difference in the CN values and the trends across the diol chain lengths is observed, suggesting that the 1st solvation shell structure is similar in all diol systems studied in the current work, and essentially independent of the diol HBD. HB number calculations carried out using TRAVIS[62,63] are provided in Table **S29** and a summary of the radial distribution functions of the HB pairs is provided in the SI in Figures **S5** and **S6**.

The denticity of chloride-diol (Cl-HO) interactions were also studied. Figure 2b shows the Cl-HO denticity for all systems at 15 mol % ChCl. Denticities at other ChCl compositions are similar and provided in Tables S9-S10. Results show that with the exception of 1,2-Eth, Cl-HO interactions are essentially monodentate in all other diol systems; the probability of bidentate interactions is calculated to be about 4-8% in 1,2-Eth depending on ChCl composition.

Examination of other ChCl:diol systems with similar OH-spaced HBDs like 1,2-butanediol and 2,3-butanediol (unpublished results) reveals that presence of bidentate Cl-HO configurations does not necessarily accompany mixing nonideality—although the probability of bidentate Cl-HO configurations is higher than that observed in 1,2-Eth at about 15%, the density of both butanediol systems project to the same value as the other longer diol systems.

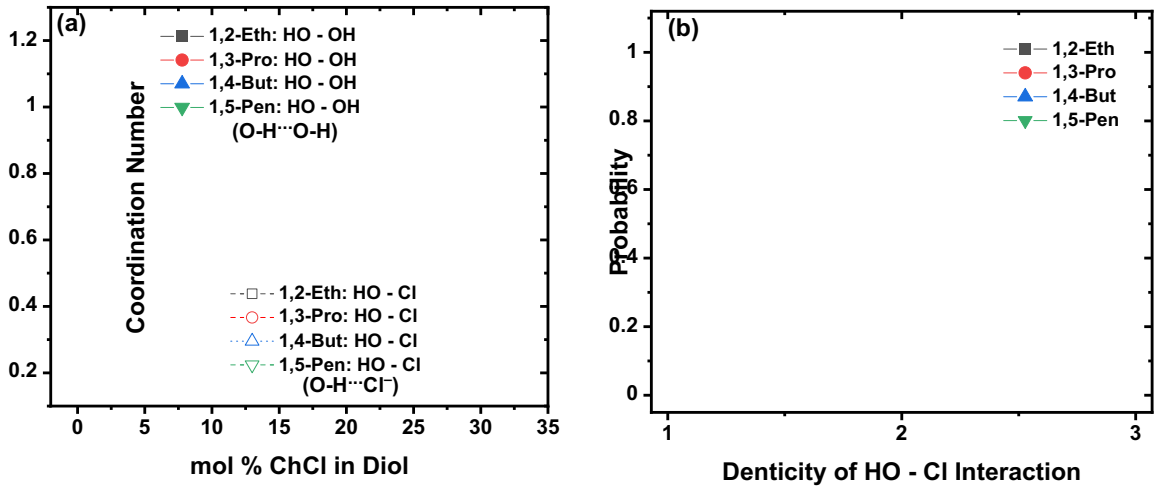

Figure 2. (a) Computed coordination numbers in the first solvation shell for the two key interaction pairs in 1,2-Eth (black squares), 1,3-Pro (red circles), 1,4-But (blue upwards-facing triangles), and 1,5-Pen (green downwards-facing triangles) systems at 298 K. The two key interaction pairs are diol hydroxyl hydrogen-diol hydroxyl hydrogen (HO-OH; closed shapes connected by straight lines; O-H···H-O interaction) and chloride-diol hydroxyl hydrogen (HO-Cl; open shapes connected by dashed lines; O-H···Cl^- interaction). Coordination numbers for 1,2-Eth and 1,3-Pro are from our previous work.[36] **(b)** Computed denticity of Cl-HO (diol) interactions in 15% ChCl simulations at 298 K.

3.3. Residence Time

While the liquid structures are similar in different diol mixtures, the interaction strength in each system can be different. One way to characterize the interaction strength computationally is to use the following correlation function:

$$C(t) = \frac{\langle h(0)h(t)\rangle}{\langle h\rangle} \quad \textbf{(2)}$$

where $h(t)$ is unity when a particular interaction is formed at time t and zero otherwise. Similar to the CN, only interactions in the first solvation shell were considered in this analysis. The residence time of the interactions were calculated by integrating **Equation (2)** as shown in **Equation (3)**:

$$\tau = \int_0^\infty C(t)\mathrm{d}t \quad \textbf{(3)}$$

The residence time is an indicator of the strength of the considered interactions, i.e., the hydrogen bonds in the DES systems. The correlation function was fitted using between 4 and 6 exponential functions as shown in **Equation (4)**[64,65]:

$$C(t) = \sum a_i e^{-t/b_i} \quad \textbf{(4)}$$

where a_i and b_i are fitting parameters, and the integration of the correlation function in Equation (3) was performed analytically over the fitting results to obtain the residence time τ. In general, six exponential functions were used; however, in some cases, the number was reduced to four when the fitted parameters became negative, resulting in unphysical estimates. The intermittent residence time, which allows reformation of interactions after they rupture, is reported rather than the continuous residence time, which does not allow the reformation of interactions.[64] **Figure 3** shows the residence times of HO-Cl interactions (τ_{HO-Cl}) increase slightly with increasing ChCl composition for 1,2-Eth and 1,3-Pro, and remain largely insensitive to ChCl composition for 1,4-But and 1,5-Pen—the large uncertainties in τ_{HO-Cl} of longer chain systems make it difficult to establish any composition-dependent trends. However, one observed chain length effect is that τ_{HO-Cl} increases exponentially with diol length (Table S11). On the other hand, much smaller uncertainties are associated with τ_{HO-OH} which exhibits different behavior for each diol system. As shown in Table S12, τ_{HO-OH} shows a slight increase with increasing ChCl composition for 1,2-Eth, remains essentially constant for 1,3-Pro, and increases upon the first addition of ChCl at 5 mol %, but subsequently decreases upon further ChCl addition for 1,4-But and 1,5-Pen. Numerical values are provided in Tables S11 and S12. Despite these systems' respective composition-dependent trends, system-specific differences are clear with the residence times of both HO-Cl and HO-OH interactions being longer in longer chain diol systems and decreasing as the diol chain gets shorter. In this regard, for both τ_{HO-Cl} and τ_{HO-OH}, 1,2-Eth are not observed to be particular outliers in system-specific trends—1,2-Eth fits the overall exponential trend of τ_{HO-Cl} and the linear trend of τ_{HO-OH}.

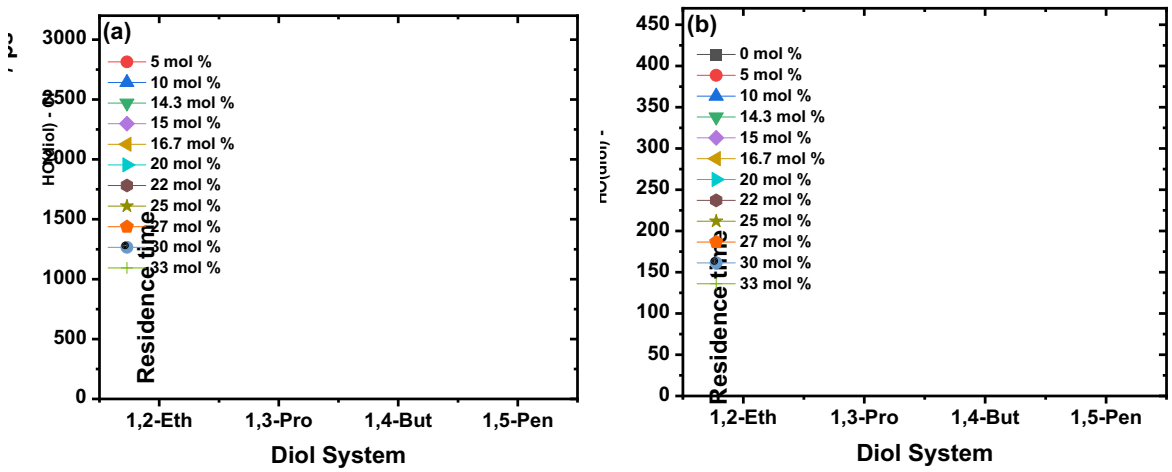

Figure 3. Computed residence times for the **(a)** OH(diol)-Cl and **(b)** OH(diol)-OH(diol) interaction pairs in each diol system. Percentages in the legend denote ChCl composition. Residence times for 1,2-Eth and 1,3-Pro systems are from our previous work.[36]

3.4. Viscosity

The viscosities for all systems are shown in **Figure 4**. Across all salt compositions, the viscosities followed the trend of 1,5-Pen > 1,4-But > 1,3-Pro > 1,2-Eth. Notably, 1,2-Eth's viscosity exponentially increases with salt concentration; the lowest value is observed at 0 mol % ChCl. On the other hand, intriguingly, 1,3-Pro, 1,4-But, and 1,5-Pen experienced a decrease in viscosity with the addition of ChCl until a minimum was reached between 5-10 mol % ChCl. Computational viscosities of the diol systems were calculated using the Green-Kubo relation:

$$\eta = \frac{V}{6k_BTV}\sum_{\alpha\leq\beta}\int_0^\infty \langle \overline{P}_{\alpha\beta}(t)\cdot\overline{P}_{\alpha\beta}(0)\rangle \, \mathrm{d}t \qquad \textbf{(5)}$$

where $\underline{P}_{\alpha\beta}$ denotes an element $\alpha\beta$ of a modified pressure tensor. The statistics of the calculated viscosity were improved by the following choice of pressure tensor elements $\overline{\mathrm{P}}_{\alpha\beta}$: $\overline{P}_{xy} = P_{xy}$, $\overline{P}_{yz} = P_{yz}$, $\overline{P}_{xz} = P_{zx}$, $\overline{P}_{xx} = 0.5\left(P_{xx} - P_{yy}\right)$, $\overline{P}_{yy} = 0.5\left(P_{yy} - P_{zz}\right)$, $\overline{P}_{zz} = 0.5(P_{xx} - P_{zz})$ where $\underline{P}_{\alpha\beta}$ represents the elements of the standard pressure tensor. The time decomposition procedure[67] was used for this calculation with 30 independent NVT simulations for each viscosity value. A bootstrap method was used to estimate the uncertainty[64] in the calculated viscosities. As seen in Figure 4, calculated viscosities show very good agreement with the experimental measurements and even the viscosity minima are captured for all but the 1,5-Pen mixture. The 1,5-Pen viscosities are slightly overestimated, and the viscosity minimum is not captured, but because the emphasis of this work is on chain length effects, the calculated viscosities were deemed

satisfactory given their agreement with the following viscosity order: 1,5-Pen > 1,4-But > 1,3-Pro > 1,2-Eth.

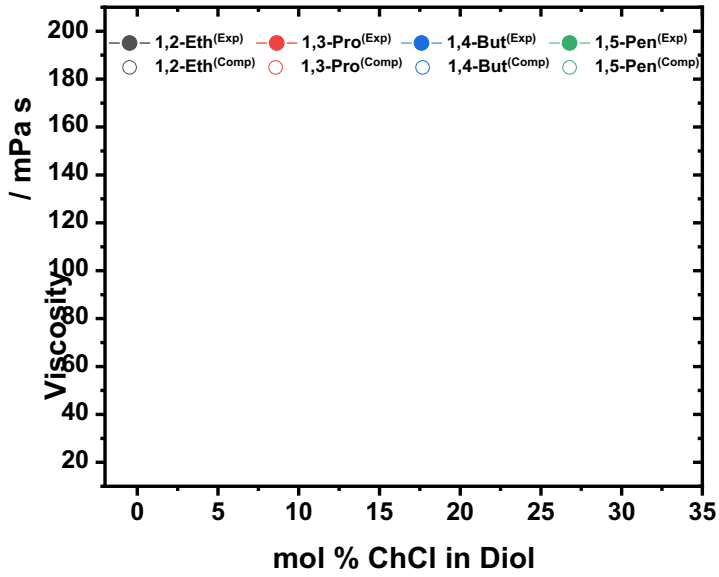

Figure 4. Viscosities (η) of 1,2-Eth (black), 1,3-Pro (red), 1,4-But (blue), and 1,5-Pen (green) binary mixtures with varying mol % of ChCl. Experimental results are shown in closed circles connected by solid lines and simulated viscosities are denoted by open circles. See Tables S13-16 for numerical values and uncertainties. T = 298 K. Experimental viscosities for 1,2-Eth are from our previous work.[35]

3.5. Solvent Relaxation Dynamics

The dynamic properties of each system were investigated experimentally by examining the relaxation dynamics of B30 dissolved in the DESs. When B30 absorbs light, its interaction with the surrounding solvent changes, prompting a reorganization of solvent molecules. This reorganization affects the time-dependent spectral changes observed for B30. Therefore, by tracking the relaxation behavior of B30, we indirectly probe the solvent relaxation dynamics and the strength of solute–solvent interactions in the system. Relaxation time constants were extracted from the fs-TA data by fitting the kinetic decay traces with a biexponential function, as shown in **Equation (6)**.

$$\mathrm{TA}(t, \lambda) = A_1 \exp(-t/\tau_1) + A_2 \exp(-t/\tau_2) + y_0 \quad \textbf{(6)}$$

A_1 and A_2 are the amplitudes, y_0 is the off-set, and τ_1 and τ_2 are the time constants. For all decay traces, the R^2 values of the fitting were greater than 0.99. The fast component, τ_1, shows a correlation with the ultrafast solvent response, while the slower component, τ_2, encompasses the slower choline rotational diffusion response.[41]

Relaxation dynamics are depicted for τ_1 (short lifetime component) and τ_2 (long lifetime component) in **Figure 5**, for each solvent system as a function of mol % ChCl. For both the fast and slow components, the 1,2-Eth system showed the smallest changes in values and overall faster relaxation than all other systems across all salt concentrations, ₂, indicating a highly mobile environment. Furthermore, the addition of ChCl led to faster solvation dynamics until ~16.67 mol % ChCl, from which point further salt addition resulted in a slowing down of dynamics. 1,3-Pro shows τ_1 and τ_2 minima in the data at ~10 mol % and ~15 mol % ChCl, respectively. 1,5-Pen also has a τ_1 minimum at ~10 mol % ChCl but has a τ_2 minimum that falls between 10-15 mol % ChCl. 1,4-But had an increase in τ_1 initially, but then decreased to a minimum at ~15 mol % ChCl. Its τ_2 component had a minimum at ~15 mol % ChCl. Across all systems, we observe that both τ_1 and τ_2 reach minima at low ChCl concentrations. This trend reflects initial disruption of the hydrogen-bond network by Cl^- ions, which makes the system more flexible. For 1,3-Pro, 1,4-But, and 1,5-Pen, we observe viscosity minima around 5–10 mol% ChCl. This overlaps with the fastest τ_1 values, reflecting the point where hydrogen-bond disruption by Cl^- temporarily makes the system more fluid.

The fast lifetime components, τ_1, were found to be relatively similar for 1,3-Pro, 1,4-But, and 1,5-Pen, while 1,2-Eth showed a different behavior (Figure 5a). This suggests that the systems with hydroxyl group spacing exhibit similar solvent response behaviors, whereas the response of 1,2-Eth is distinct from the others. In terms of τ_2, the behaviors of 1,4-But and 1,5-Pen were similar (Figure 5b), implying that these two systems have a comparable hydrogen-bonding network that slows down choline similarly due to their longer alkyl chains compared to the other diols. Moreover, the τ_1 lifetime of solvent response did not significantly vary with the 1,2-Eth system. A similar observation was made for τ_2. The addition of ChCl had a lesser impact on the properties of 1,2-Eth compared to the other systems that had spacing between hydroxyl groups. This behavior is likely related to the weaker interactions among components in 1,2-Eth, as shown in the lower density of the mixtures relative to ideal mixing as shown in Figure 1b.

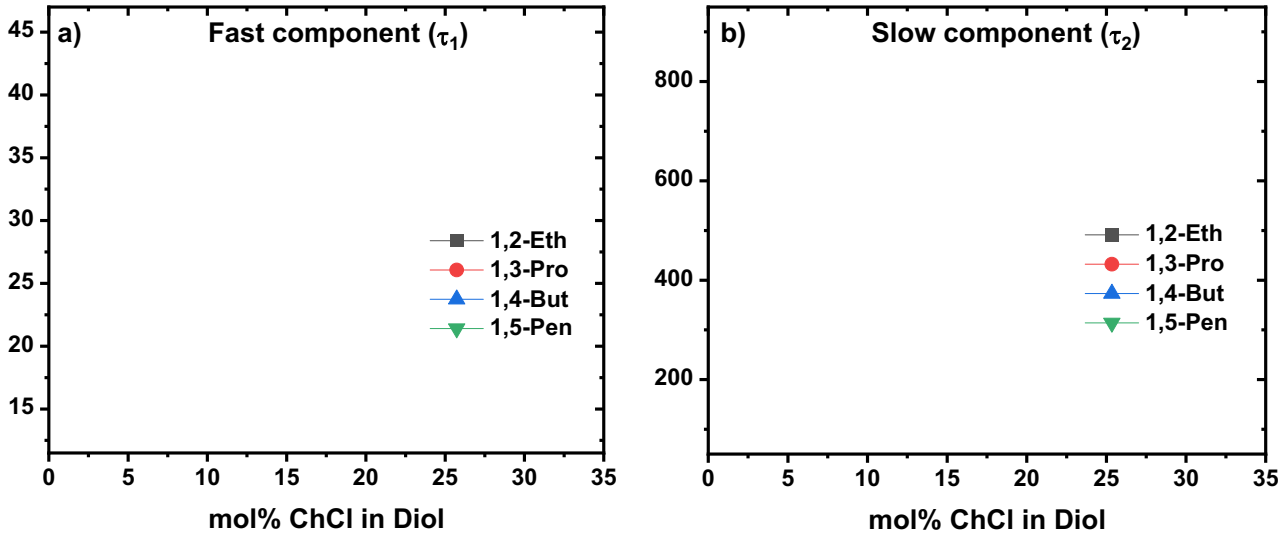

Figure 5. Time constants of **(a)** fast relaxation component τ_1 and **(b)** slow relaxation component τ_2 of binary diol mixtures 1,2-Eth (black squares), 1,3-Pro (red circles), 1,4-But (upwards-facing blue triangles), and 1,5-Pen (downwards-facing green triangles) as a function of mol % ChCl. Data points were acquired by biexponential fitting using Equation (6) around peak maxima (λ_{fitted} = 500-650 nm). T = 298 K. See Tables S17-S20 for numerical values and uncertainties. Dynamics for 1,2-Eth and 1,3-Pro are from our previous work.[36,66]

3.6. Self-Diffusion Coefficients

Self-diffusion is another important solvent characteristic that can help understand solvent behavior. Self-diffusion coefficients of the diol and choline components in each system were measured experimentally by pulsed-field gradient NMR and are summarized in **Figure 6**. Figure 6a shows that in all diol systems and across all compositions, choline is the slowest-moving species, with the diol being the most mobile. The diffusivity of chloride (^{35}Cl) was not obtained experimentally due to rapid signal decay from strong quadrupolar relaxation and extremely short T_2, which prevents signal acquisition within the diffusion NMR timescale. In all systems but 1,5-Pen, the diffusivity of all species decreases as more ChCl is added. For 1,5-Pen, diffusivity increases from 5 mol % ChCl to 10 mol % ChCl and then decreases again at 20 mol %. The difference between the self-diffusivity of choline and diol molecules is observed to decrease as diol chain length increases. Experimental and computational values for self-diffusion are provided in Tables S21-S28.

The self-diffusion coefficients of each species in the simulations were calculated using the Einstein relation, **Equation (7)**:

$$D_s = \frac{1}{6}\lim_{t\to\infty}\frac{\mathrm{d}}{\mathrm{d}t}\frac{1}{N}\sum_{i=1}^{N}\langle|\boldsymbol{r}_i(t)-\boldsymbol{r}_i(0)|^2\rangle \quad \textbf{(7)}$$

where $\boldsymbol{r}_i(t)$ is the center of mass (COM) position of species i at time t and N is the number of individual species. Self-diffusivities were computed from the Einstein relation, using 30 independent trajectories for each composition of every diol system. For each trajectory, the relation was evaluated over 4 ns for 1,2-Eth and 1,3-Pro, 9 ns for 1,4-But, and 19 ns for 1,5-Pen to ensure that each system reached the linear, diffusive regime. Bootstrap sampling was carried out using the 30 relations and the reported value for each composition is the mean of the bootstrapped distribution. System size corrections were applied using the method outlined by Yeh and Hummer.[67,68] Figure 6b shows the calculated self-diffusion coefficient of all species in each diol system as a function of ChCl composition. It was observed that all species across all chain lengths diffuse more slowly with increasing ChCl composition. Comparison with experimental results shows that simulations are in excellent agreement with the NMR measurements. The diffusivities of the respective systems decrease as their chain lengths increase, resulting in the following diffusivity order consistent with the trend of viscosity: 1,2-Eth > 1,3-Pro > 1,4-But > 1,5-Pen. In all systems but 1,4-But, chloride is faster than the diol until their diffusivities cross at about 15 mol % ChCl, after which the diol becomes the more mobile component. In the case of 1,4-But, this crossing of chloride and diol diffusivity occurs at 20% which is the last composition at which the longer chain diols are in liquid phase. Choline is the slowest moving species in all four diol systems regardless of composition, and the diffusivity of chloride gradually converges to the diffusivity of choline as ChCl composition increases in all systems. As was also noted in the experimental measurements, the difference between the self-diffusivities of choline and diol molecules within the same DES decreases as the diol chain length gets longer. This effect is most substantial in 1,2-Eth, followed by 1,3-Pro, 1,4-But, and 1,5-Pen in that order.

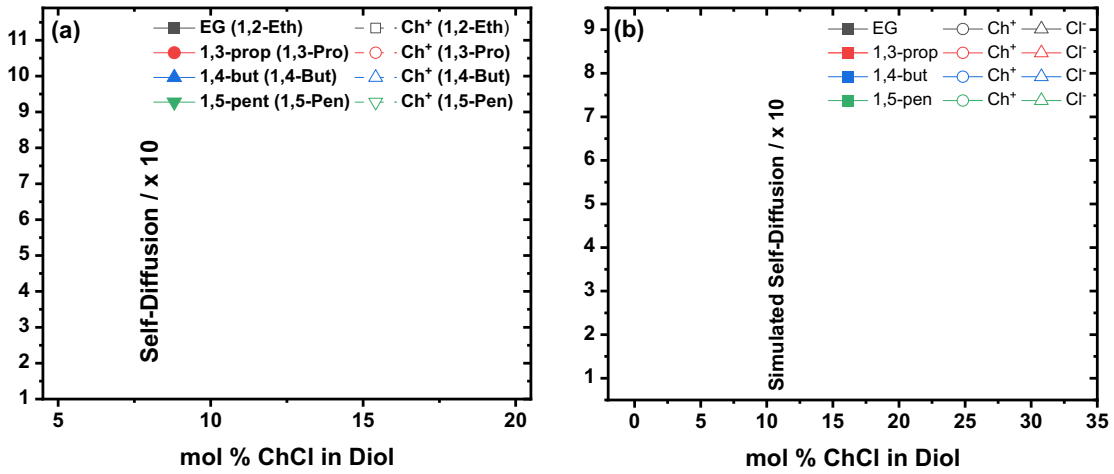

Figure 6. (**a**) Self-diffusion coefficients measured experimentally by pulsed-field NMR techniques for 1,2-Eth (black squares), 1,3-Pro (red circles), 1,4-But (blue upwards-facing triangles), and 1,5-Pen (green downwards-facing triangles). Self-diffusion of diol solvent is denoted in solid shapes connected by solid lines, while the self-diffusion of choline in each mixture is denoted by open shapes and connected by dashed lines. Composition ranges from 5 to 20 mol % ChCl in diols. (**b**) Self-diffusion coefficients calculated from simulations for 1,2-Eth (black), 1,3-Pro (red), 1,4-But (blue), and 1,5-Pen (green) systems. The diol solvents are depicted by closed squares, choline is depicted by open circles, and chloride is depicted by open triangles. $T = 298$ K. The computed self-diffusion coefficients for 1,2-Eth and 1,3-Pro are from our previous work.[36] See Tables S21-S28 for numerical experimental and computed self-diffusion coefficient values.

3.7. Conductivity and Ionicity

Ionic conductivities were both measured and computed as a function of mol % ChCl. The measured conductivities, as depicted in Figure 7a, displayed an increase upon the addition of ChCl at low ChCl concentration for all examined systems. Notably, the 1,2-Eth system exhibited the most pronounced increase in conductivity, which rose linearly until ~15 mol % ChCl, after which it reached a maximum and eventually started decreasing beyond ~25 mol % ChCl. The initial conductivity increase is attributed to an increase in charge carriers, but further salt addition increased viscosity, leading to a reduction in the mobility of the ions. This is likely the cause of the plateauing and subsequent decrease of conductivity.[1,69,70] Similarly, the 1,3-Pro system displayed a mostly linear increase in conductivity until ~20 mol % ChCl, followed by a plateau between ~20-25 mol % ChCl and likely a decrease beyond 30 mol %. The conductivities of 1,4-But and 1,5-Pen systems exhibited shallower increases. In comparison, across all salt compositions (excluding salt-less systems), the conductivities ranked in the order of 1,2-Eth > 1,3-Pro > 1,4-But > 1,5-Pen.

Conductivities were calculated from MD using the following Einstein relation

$$\sigma_E = \frac{1}{6k_BTV}\lim_{t\to\infty}\frac{\mathrm{d}}{\mathrm{d}t}\langle\sum_{i=1}^{N_{\mathrm{ChCl}}}\sum_{j=1}^{N_{\mathrm{ChCl}}} q_i q_j[\boldsymbol{r}_i(t)-\boldsymbol{r}_i(0)]\cdot[\boldsymbol{r}_j(t)-\boldsymbol{r}_j(0)]\rangle \quad \textbf{(8)}$$

where k_B is Boltzmann's constant, T is temperature, V is the system volume, N_i is the number of species i, q_i is the charge of species i, and $r_i(t)$ is the COM position of species i at time t. The ionic conductivity was obtained by adapting the time decomposition method.[71] For each system, 30 independent 20 ns trajectories were generated in the NVT ensemble. Equation (8) was applied to each trajectory and the average is reported as the final conductivity value, with the uncertainty calculated using the bootstrap method. As observed in **Figure 7**, ionic conductivities calculated from simulations agree extremely well with the experimental measurements with a maximum deviation of about 17%. The respective magnitudes of conductivities are captured perfectly with the same order: 1,2-Eth > 1,3-Pro > 1,4-But > 1,5-Pen.

Another method to examine the solvent conductivity is to consider the ionic correlation effects via their ionicities, or inverse Haven ratios. Ionicity, σ_E/σ_{NE}, is the ratio of the Einstein conductivity to the Nernst-Einstein conductivity; it quantifies the extent of dissociation of ions. The Einstein conductivity was calculated using **Equation (8)** as detailed above, and the Nernst-Einstein conductivity was calculated using the following expression

$$\sigma_{NE} = \frac{N_{ChCl}}{Vk_BT}(q_{Ch^+}^2 D_{Ch^+} + q_{Cl^-}^2 D_{Cl^-}) \quad \textbf{(9)}$$

where previously calculated self-diffusion coefficients of each species, D_i, were used. σ_{NE} omits the ionic correlation contribution terms found in Equation 8. An ionicity of 1 indicates that the solvated ions are completely dissociated and there is no ionic correlation. Ionicities less than 1 indicate correlation of ions—the movement of ions is correlated to some extent. As seen in Figure 7b, all systems show varying ionicities with both diol chain length and ChCl composition; ionicities are less than unity for most systems. Uncertainties are high due to substantial noise in the ionic correlation functions. Ionic correlations are stronger in 1,5-Pen across all compositions, but no clear trends are observed in 1,3-Pro or 1,4-But as a function of ChCl fraction. Ionic correlations are observed to increase with increasing ChCl composition in the case of 1,2-Eth.

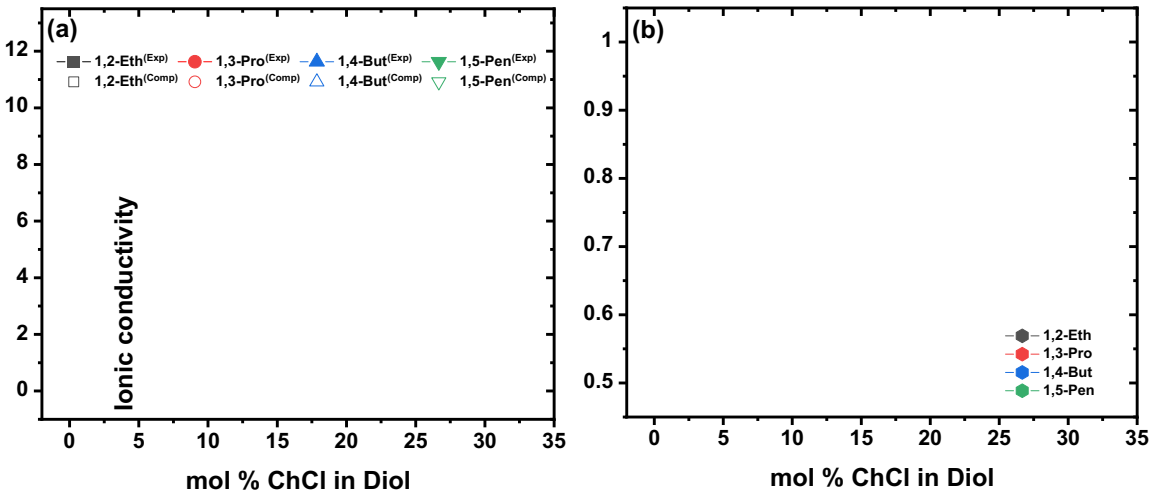

Figure 7. (**a**) Ionic conductivities (σ) of 1,2-Eth (black squares), 1,3-Pro (red circles), 1,4-But (blue upwards triangles), and 1,5-Pen (green downwards triangles) binary mixtures with varying mol % of ChCl. Experimental results are shown in closed shapes and connected by solid lines. Simulation conductivity values are denoted by open shapes. See Tables S13-S16 for numerical values and uncertainties. T = 298 K. Ionic conductivities for the 1,3-Pro system were taken from our previous work.[36] (**b**) Ionicity as a function of mol % ChCl for 1,2-Eth (black), 1,3-Pro (red), 1,4-But (blue), and 1,5-Pen (green).

3.8. Ionic Conductivity Contributions

Based on **Equation (8)**, the Einstein conductivity can be divided into species-wise contributions. A breakdown of the ionic conductivity contributions allows us to quantify the impact of ionic correlations and determine which ionic correlations enhance or hinder overall charge transport. In the breakdown shown in Figure 8, the sum of the Ch and Cl self-terms would be the total ionic conductivity if we assumed an ionicity of 1, i.e., if the ions were completely uncorrelated. The various distinct (Ch-Ch and Cl-Cl) and cross (Ch-Cl) terms make either positive or negative contributions to the total conductivity and are important components of the bulk conductivity. All self-terms initially make increasingly positive contributions to the conductivity as ChCl composition increases. This is expected, because the population of the charged species increases with increasing amounts of ChCl. At high ChCl compositions, the same self-term contributions plateau due to lower ionic mobility caused by higher solvent viscosity. Species-wise contributions also give a more detailed picture of how ionic correlation changes. The Ch-Cl cross-term makes a slightly positive contribution in the shorter chain systems 1,2-Eth and 1,3-Pro, but begins to make negative contributions in the longer chain systems 1,4-But and 1,5-Pen. This change in conductivity contribution reflects stronger correlation between Ch and Cl ions

accompanying diol chain elongation—negative contributions indicating ionic movements detrimental to overall charge transport and positive contributions indicating ionic movement beneficial to overall charge transport. This suggests that Ch-Cl ionic correlations are strongest in longer chain systems such as 1,5-Pen and weakest in shorter chain systems such as 1,2-Eth. This observation is consistent with the chelating tendency and unusual mixing of the 1,2-Eth systems, as discussed earlier.

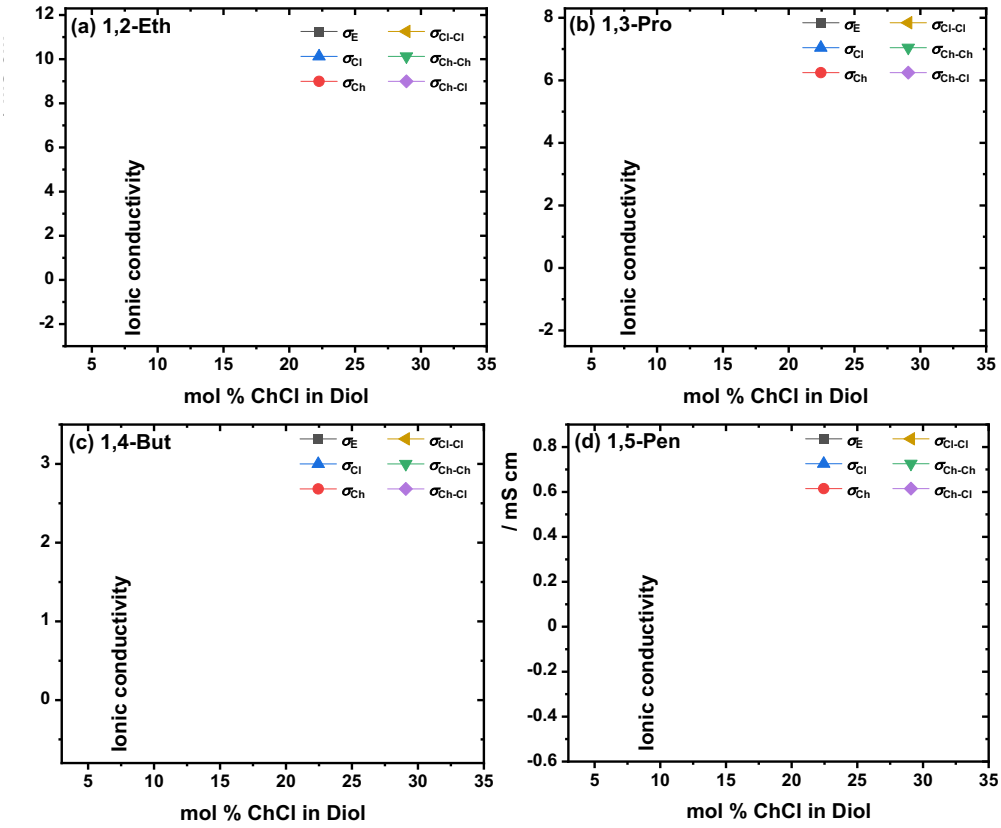

Figure 8. Ionic conductivity contributions calculated using Equation (8) plotted for (**a**) 1,2-Eth, (**b**) 1,3-Pro, (**c**) 1,4-But, and (**d**) 1,5-Pen systems at 298 K. 1,4-But and 1,5-Pen systems were cut off at 20 mol % ChCl since they are not purely liquid beyond the 20 mol % ChCl composition.

3.9. Polarity

The determination of polarity was achieved using Reichardt's dye B30 as a probe molecule to measure the absorbance maximum and the $E_T(30)$ scale, established by Reichardt.[39,53] **Equation (10)** was used to obtain the $E_T(30)$ values, where the primary variable required is λ_{max}, the wavelength of maximum absorption. For B30, this corresponds to the longest-wavelength CT absorption band, which reflects the lowest-energy electronic transition (Scheme 1). Notably, B30 is negatively solvatochromic by nature, causing a hypsochromic shift (blueshift) as the polarity of

the solvent increases. Planck's constant (h), speed of light (c), and Avogadro's number (N_A) are among the other terms in the equation, but they are constants.[39,72,73]

$$E_T(30)\ (\text{kcal mol}^{-1}) = h\ c\ N_A\ \nu_{max} = 28591 / \lambda_{max} \quad \textbf{(10)}$$

$E_T(30)$ values were obtained for all systems by determining λ_{max} using UV-vis spectroscopy (**Figure 9**). Across all systems and salt concentrations, the polarity trend followed the order of 1,2-Eth > 1,3-Pro > 1,4-But > 1,5-Pen. While polarity increased with increasing mol % ChCl for all systems, the rate of increase slowed down after ~15 mol % ChCl. Among the systems, 1,2-Eth was the least sensitive to salt addition, exhibiting lower overall changes in $E_T(30)$ with increasing ChCl content than 1,3-Pro, 1,4-But, and 1,5-Pen. The polarity response of each system was determined by calculating the percentage change in $E_T(30)$ relative to pure diol, as illustrated in Figure 9b. The trend observed was that systems with longer alkyl chain lengths exhibited greater sensitivity to the addition of ChCl.

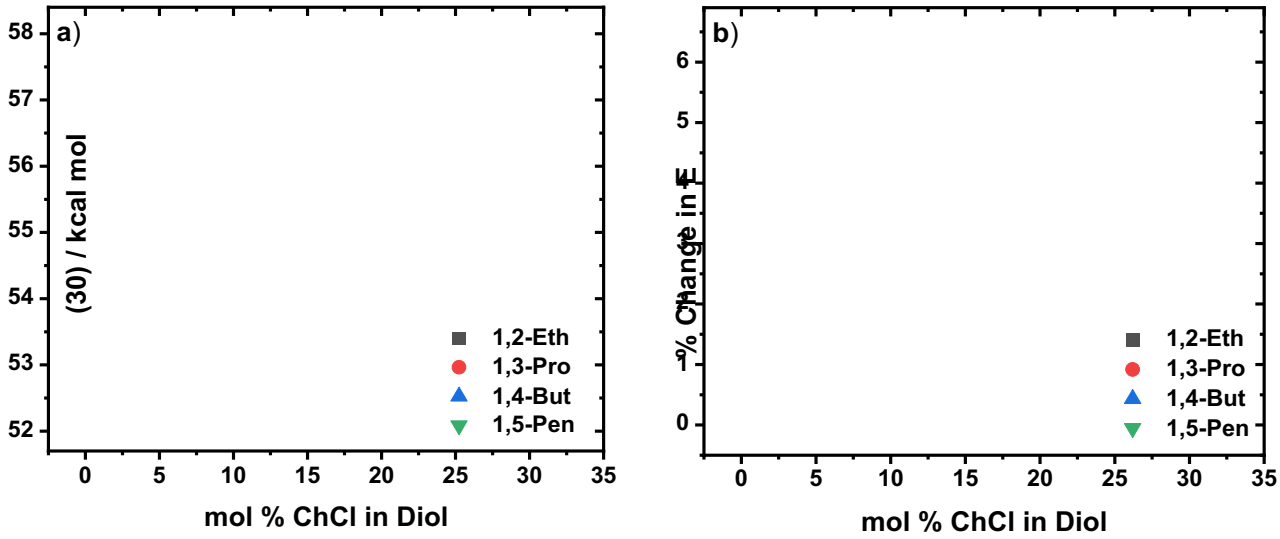

Figure 9. (a) $E_T(30)$ polarity as a function of mol % ChCl in binary diol mixtures for 1,2-Eth (black squares), 1,3-Pro (red circles), 1,4-But (blue upwards-facing triangles), and 1,5-Pen (green downwards-facing triangles). **(b)** depicts the % change in $E_T(30)$ polarity of binary mixtures compared to pure diols as a function of mol % ChCl in diol. A small amount of betaine-30 was dissolved in each system. T = 298 K. See Tables S17-S20 for numerical values. $E_T(30)$ values for 1,2-Eth and 1,3-Pro systems were from our previous work.[36]

3.10. Static Dielectric Constant

The static dielectric constant of each system was calculated from the simulations. To calculate the dielectric constant, the approach used by Seal and coworkers[74] was employed, which uses the following **Equation (11)**:

$$\epsilon = 1 + \frac{\langle \boldsymbol{M}^2 \rangle - \langle \boldsymbol{M} \rangle^2}{3Vk_BT\epsilon_0} \quad \textbf{(11)}$$

where $\boldsymbol{M}$ denotes the sum of all dipole moments in the simulation cell, the brackets $\langle \quad \rangle$ denote the time average, and ϵ_0 is the permittivity of free space. Static dielectric constant is a measure of how well the solvent can screen an applied electric field—higher static dielectric constants indicate that the solvent has a stronger effect to screen the Coulombic interactions between ionic species and therefore better accommodate polar species. **Figure 10** shows that the calculated static dielectric constants for the pure diols follow the trend 1,2-Eth > 1,3-Pro > 1,4-But > 1,5-Pen, consistent with literature values[75] although the values are underestimated by the calculation. For a given diol, the static dielectric constant decreases with increasing ChCl composition, a similar trend observed experimentally in glyceline by Spittle et al.[76] At a given ChCl composition, the calculated static dielectric constant follows the same order as in the pure diol: 1,2-Eth > 1,3-Pro > 1,4-But > 1,5-Pen, indicating weaker ion-ion interactions in shorter alkyl chain systems due to the stronger screening effect. This is consistent with observations discussed in earlier sections.

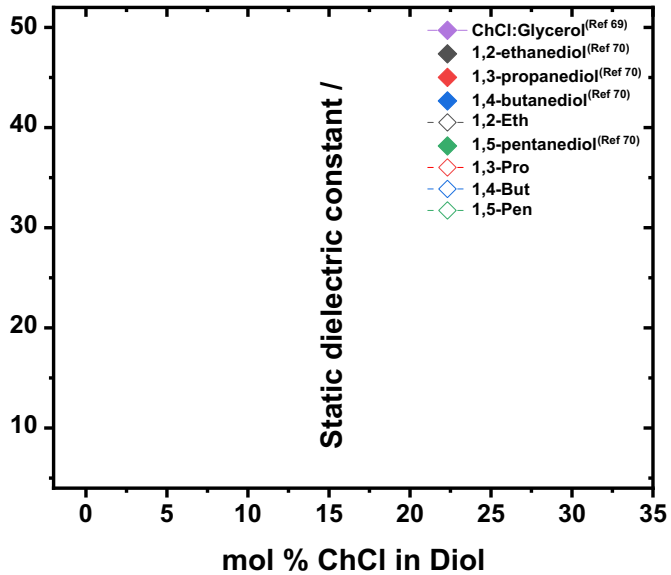

Figure 10. Static dielectric constants calculated at 298 K for all systems as a function of mol % ChCl. Open diamonds connected by dashed lines denote computational results from this work for 1,2-Eth (black), 1,3-Pro (red), 1,4-But (blue), and 1,5-Pen (green). Closed black, red, blue, and green diamonds denote

experimental values of pure diols (EG, 1,3-propanediol, 1,4-butanediol, and 1,5-pentanediol, respectively) obtained from the CRC Handbook of Chemistry and Physics.[75] Experimental values for ChCl:glycerol mixtures at 250 K were obtained from the literature.[76]

4. Conclusion

The aim of this study was to investigate how the chain length of different glycols in deep eutectic solvents (DESs) affects their dynamics and solvation properties, including the conductivity, viscosity, density, polarity, solvation structure, and solvation dynamics. Four different DES systems were investigated. Classical molecular dynamics simulations were employed to obtain deeper mechanistic insights. The simulation results matched the experimentally measured properties very well and were used to investigate the detailed solvent structure and dynamics. The results revealed that 1,2-Eth had the highest conductivity, followed by 1,3-Pro, whereas 1,4-But and 1,5-Pen had similar conductivities. For viscosity, 1,2-Eth exhibited a continuous increase with the addition of ChCl, while 1,3-Pro, 1,4-But, and 1,5-Pen showed a viscosity minimum at 5-10 mol % ChCl. All systems exhibited an increase in density with increasing salt concentration, with 1,2-Eth having the highest density and the smallest change in density across all salt concentrations. In general, smaller alkyl chains led to higher conductivity, lower viscosity, and higher density. Regarding polarity, 1,2-Eth had the lowest sensitivity to salt addition compared to other systems, but it had the highest polarity across all salt concentrations. The trend was that polarity decreased as the alkyl chain length increased. The systems containing hydroxyl spacing all had similar τ_1 responses. Their solvent responses were similar to each other but distinct from 1,2-Eth. For the τ_2 response, 1,4-But and 1,5-Pen had similar lifetimes, likely due to their lengthy alkyl chains that caused the slower diffusional dynamics measured. A closer look at the solvation environments revealed that all systems have similar local structures up to their first solvation shell, indicating similar arrangement of immediate hydrogen-bonding interactions. Due to various factors, such as viscosity, steric effects, and hydrogen-bonding affinities, the strength of key interactions is proportional to the chain length of the HBDs in their respective systems—longer interaction residence times are observed in longer chain HBD systems. Ion interactions were examined and found to increase as HBD chain length increases, being weakest in 1,2-Eth, consistent with the trend in static dielectric constant. The unusual mixing observed in 1,2-Eth is consistent with this weaker ionic correlation and faster solvent response (τ_1). The spacing between

hydroxyl groups present in the glycolic HBDs, largely determined the dynamics of DESs, producing a scaling-like effect on key properties such as viscosity, conductivity, self-diffusion coefficients. This work suggests that small diols are good candidates for DESs due to their favorable dynamic and transport properties, making them suitable for applications in energy storage and electrolyte transport. On the contrary, larger diols are more apolar and slower in solvation dynamics, and likely less competitive for electrochemical energy storage applications.

Acknowledgments

This research was funded by the Breakthrough Electrolytes for Energy Storage Energy Frontier Research Center (BEES2 EFRC), supported by the Basic Energy Sciences program, U.S. Department of Energy, Office of Science (Award # DE-SC0019409). CB expresses gratitude to CWRU for supporting the Center for Chemical Dynamics and Nanomaterials Research. DK, YZ, and EM thank the Center for Research Computing (CRC) at the University of Notre Dame for providing computational resources.

References

[1] A.P. Abbott, D. Boothby, G. Capper, D.L. Davies, R.K. Rasheed, Deep eutectic solvents formed between choline chloride and carboxylic acids: versatile alternatives to ionic liquids, J. Am. Chem. Soc. 126 (2004) 9142–9147.

[2] A.P. Abbott, G. Capper, D.L. Davies, R.K. Rasheed, V. Tambyrajah, Novel solvent properties of choline chloride/urea mixtures, Chem. Commun. (2003) 70–71.

[3] J. Wu, Q. Liang, X. Yu, L. Qiu-Feng, L. Ma, X. Qin, G. Chen, B. Li, Deep eutectic solvents for boosting electrochemical energy storage and conversion: a review and perspective, Adv. Funct. Mater. 31 (2021).

[4] Q. Zhang, K. de Oliveira Vigier, S. Royer, F. Jérôme, Deep eutectic solvents: syntheses, properties and applications, Chem. Soc. Rev. 41 (2012) 7108–7146.

[5] E.L. Smith, A.P. Abbott, K.S. Ryder, Deep eutectic solvents (DESs) and their applications, Chem. Rev. 114 (2014) 11060–11082.

[6] D.V. Wagle, H. Zhao, G.A. Baker, Deep eutectic solvents: sustainable media for nanoscale and functional materials, Acc. Chem. Res. 47 (2014) 2299–2308.

[7] G. García, S. Aparicio, R. Ullah, M. Atilhan, Deep eutectic solvents: physicochemical properties and gas separation applications, Energy Fuels 29 (2015) 2616–2644.

[8] B.B. Hansen, S. Spittle, B. Chen, D. Poe, Y. Zhang, J.M. Klein, A. Horton, L. Adhikari, T. Zelovich, B.W. Doherty, B. Gurkan, E.J. Maginn, A. Ragauskas, M. Dadmun, T.A. Zawodzinski, G.A. Baker, M.E. Tuckerman, R.F. Savinell, J.R. Sangoro, Deep eutectic solvents: a review of fundamentals and applications, Chem. Rev. 121 (2021) 1232–1285.

[9] A.Z. Weber, M.M. Mench, J.P. Meyers, P.N. Ross, J.T. Gostick, Q. Liu, Redox flow batteries: a review, J. Appl. Electrochem. 41 (2011) 1137–1164.

[10] P. Alotto, M. Guarnieri, F. Moro, Redox flow batteries for the storage of renewable energy: a review, Renew. Sustain. Energy Rev. 29 (2014) 325–335.

[11] M.R. Mohamed, S.M. Sharkh, F.C. Walsh, Redox flow batteries for hybrid electric vehicles: progress and challenges, in: 5th IEEE Vehicle Power and Propulsion Conference, VPPC '09, 2009, pp. 551–557.

[12] I. Bakó, T. Grósz, G. Pálinkás, M.C. Bellissent-Funel, Ethylene glycol dimers in the liquid phase: a study by X-ray and neutron diffraction, J. Chem. Phys. 118 (2003) 3215–3221.

[13] P. Das, P.K. Das, E. Arunan, Conformational stability and intramolecular hydrogen bonding in 1,2-ethanediol and 1,4-butanediol, J. Phys. Chem. A 119 (2015) 3710–3720.

[14] F. Kollipost, K.E. Otto, M.A. Suhm, A symmetric recognition motif between vicinal diols: the fourfold grip in ethylene glycol dimer, Angew. Chem. 128 (2016) 4667–4671.

[15] D.V. Wagle, C.A. Deakyne, G.A. Baker, Quantum chemical insight into the interactions and thermodynamics present in choline chloride based deep eutectic solvents, J. Phys. Chem. B 120 (2016) 6739–6746.

[16] P. Kalhor, J. Xu, H. Ashraf, B. Cao, Z.W. Yu, Structural properties and hydrogen-bonding interactions in binary mixtures containing a deep-eutectic solvent and acetonitrile, J. Phys. Chem. B 124 (2020) 1229–1239.

[17] J. Cerar, A. Jamnik, M. Tomšič, Supra-molecular structure and rheological aspects of liquid terminal 1,n-diols from ethylene glycol to 1,5-pentanediol, J. Mol. Liq. 276 (2019) 307–317.

[18] Y. Zhang, D. Poe, L. Heroux, H. Squire, B.W. Doherty, Z. Long, M. Dadmun, B. Gurkan, M.E. Tuckerman, E.J. Maginn, Liquid structure and transport properties of the deep eutectic solvent ethaline, J. Phys. Chem. B 124 (2020) 5251–5264.

[19] A. Yadav, J.R. Kar, M. Verma, S. Naqvi, S. Pandey, Densities of aqueous mixtures of (choline chloride + ethylene glycol) and (choline chloride + malonic acid) deep eutectic solvents in temperature range 283.15–363.15 K, Thermochim. Acta 600 (2015) 95–101.

[20] F.S. Mjalli, O.U. Ahmed, Physical properties and intermolecular interaction of eutectic solvents binary mixtures: reline and ethaline, Asia-Pac. J. Chem. Eng. 11 (2016) 549–557.

[21] V. Alizadeh, F. Malberg, A.A.H. Pádua, B. Kirchner, Are there magic compositions in deep eutectic solvents? Effects of composition and water content in choline chloride/ethylene glycol from ab initio molecular dynamics, J. Phys. Chem. B 124 (2020) 7433–7443.

[22] A. Gaur, S. Balasubramanian, Liquid ethylene glycol: prediction of physical properties, conformer population and interfacial enrichment with a refined non-polarizable force field, Phys. Chem. Chem. Phys. 24 (2022) 10985–10992.

[23] N.F. Gajardo-Parra, V.P. Cotroneo-Figueroa, P. Aravena, V. Vesovic, R.I. Canales, Viscosity of choline chloride-based deep eutectic solvents: experiments and modeling, J. Chem. Eng. Data 65 (2020) 5581–5592.

[24] H. Wang, S. Liu, Y. Zhao, J. Wang, Z. Yu, Insights into the hydrogen bond interactions in deep eutectic solvents composed of choline chloride and polyols, ACS Sustain. Chem. Eng. 7 (2019) 7760–7767.

[25] L.H. Xu, D. Wu, M. Zhong, G.B. Wang, X.Y. Chen, Z.J. Zhang, Construction of a new deep eutectic solvent system based on choline chloride and butanediol: influence of hydroxyl position on structure and supercapacitor performance, J. Power Sources 490 (2021).

[26] O.E. Plastiras, V. Samanidou, Applications of deep eutectic solvents in sample preparation and extraction of organic molecules, Molecules 27 (2022).

[27] Z.S. Othman, N.H. Hassan, S.I. Zubairi, Alcohol-based deep eutectic solvent as a green additive to increase rotenone yield, AIP Conf. Proc. (2015).

[28] X. Deng, X. Duan, L. Gong, D. Deng, Ammonia solubility, density, and viscosity of choline chloride–dihydric alcohol deep eutectic solvents, J. Chem. Eng. Data 65 (2020) 4845–4854.

[29] L.P. Kuhn, The Hydrogen Bond. I. Intra- and Intermolecular Hydrogen Bonds in Alcohols, Cornell University Press, 1952.

[30] M. Tomšič, J. Cerar, A. Jamnik, Characterization of the supramolecular assembly in 1,4-butanediol, J. Mol. Liq. 259 (2018) 291–303.

[31] H.Y. Chen, Y.L. Cheng, K. Takahashi, Theoretical calculation of OH vibrational overtone spectra of 1,5-pentanediol and 1,6-hexanediol, J. Phys. Chem. A 115 (2011) 14315–14324.

[32] A.G. Petrov, The Lyotropic State of Matter, Gordon and Breach Science Publishers, 1999.

[33] A.G.M. Ferreira, A.P.V. Egas, I.M.A. Fonseca, A.C. Costa, D.C. Abreu, L.Q. Lobo, The viscosity of glycerol, J. Chem. Thermodyn. 113 (2017) 162–182.

[34] M.K. Alomar, M. Hayyan, M.A. Alsaadi, S. Akib, A. Hayyan, M.A. Hashim, Glycerol-based deep eutectic solvents: physical properties, J. Mol. Liq. 215 (2016) 98–103.

[35] R. Pandian, B.B. Hansen, G. de Araujo Lima e Souza, J.R. Sangoro, S. Greenbaum, C. Burda, Tuning solvation dynamics of electrolytes at their eutectic point through halide identity, Molecules 30 (2025) 2113.

[36] R. Pandian, D. Kim, Y. Zhang, I. Alfurayj, D.M. Prado, E. Maginn, C. Burda, Chain length and OH-spacing effects on diol-based deep eutectic solvents, J. Mol. Liq. 393 (2024) 123534.

[37] M.C. Beard, G.M. Turner, C.A. Schmuttenmaer, Measuring intramolecular charge transfer via coherent generation of THz radiation, J. Phys. Chem. A 106 (2002) 878–883.

[38] Š. Budzák, T. Jaunet-Lahary, A.D. Laurent, C. Laurence, M. Medved', D. Jacquemin, Exploring the solvatochromism of betaine-30 with ab initio tools: from accurate gas-phase calculations to solvation models, Chem. Eur. J. 23 (2017) 4108–4119.

[39] C. Reichardt, Polarity of ionic liquids determined empirically using solvatochromic pyridinium N-phenolate betaine dyes, in: Green Chem., RSC, 2005, pp. 339–351.

[40] J. Lobaugh, P.J. Rossky, Solvent and intramolecular effects on the absorption spectrum of betaine-30, J. Phys. Chem. A 104 (2000) 899–907.

[41] I. Alfurayj, C.C. Fraenza, Y. Zhang, R. Pandian, S. Spittle, B. Hansen, W. Dean, B. Gurkan, R. Savinell, S. Greenbaum, E. Maginn, J. Sangoro, C. Burda, Solvation dynamics of wet ethaline: water is the magic component, J. Phys. Chem. B 125 (2021) 8888–8901.

[42] J.P. Cerón-Carrasco, D. Jacquemin, C. Laurence, A. Planchat, C. Reichardt, K. Sraïdi, Determination of a solvent hydrogen-bond acidity scale using solvatochromism of pyridinium-N-phenolate betaine dye 30 and PCM-TD-DFT, J. Phys. Chem. B 118 (2014) 4605–4614.

[43] R. Pandian, H. Burda, I. Alfurayj, C. Reichardt, C. Burda, 60 years of betaine-30—from solvatochromic discovery to future frontiers, J. Phys. Chem. B 128 (2024) 6990–7001.

[44] M. Maroncelli, Computer simulations of the solvatochromism of betaine-30, J. Phys. Chem. B 103 (1999) 7704–7719.

[45] P.J. Reid, P.F. Barbara, Dynamic solvent effect on betaine-30 electron-transfer kinetics in alcohols, 1995.

[46] R. Scholz, M. Darwish, M. Schreiber, Ultrafast electron transfer of betaine-30, J. Lumin. 76–77 (1998) 404–407.

[47] M.L. Horng, J.A. Gardecki, A. Papazyan, M. Maroncelli, Subpicosecond measurements of polar solvation dynamics: Coumarin 153 revisited, 1995.

[48] S.A. Kovalenko, N. Eilers-König, T.A. Senyushkina, N.P. Ernsting, Charge transfer and solvation of betaine-30 in polar solvents: a femtosecond transient absorption study, J. Phys. Chem. A 105 (2001) 4834–4843.

[49] C.C. Fraenza, R.A. Elgammal, M.N. Garaga, S. Bhattacharyya, T.A. Zawodzinski, S.G. Greenbaum, Dynamics of glyceline and interactions of constituents: a multitechnique NMR study, J. Phys. Chem. B 126 (2022) 890–905.

[50] J.P. Cerón-Carrasco, D. Jacquemin, C. Laurence, A. Planchat, C. Reichardt, K. Sraïdi, Solvent polarity scales: determination of new ET(30) values for 84 organic solvents, J. Phys. Org. Chem. 27 (2014) 512–518.

[51] D.J. Eyckens, L.C. Henderson, A review of solvate ionic liquids: physical parameters and synthetic applications, Front. Chem. 7 (2019).

[52] D.V. Matyushov, R. Schmid, B.M. Ladanyi, A thermodynamic analysis of the π* and ET(30) polarity scales, 1997.

[53] C. Reichardt, Solvatochromic dyes as solvent polarity indicators, Chem. Rev. 94 (1994) 2319–2358.

[54] E.O. Stejskal, J.E. Tanner, Spin diffusion measurements: spin echoes in the presence of a time-dependent field gradient, J. Chem. Phys. 42 (1965) 288–292.

[55] S. Plimpton, Fast parallel algorithms for short-range molecular dynamics, J. Comput. Phys. 117 (1995) 1–19.

[56] J. Wang, R.M. Wolf, J.W. Caldwell, P.A. Kollman, D.A. Case, Development and testing of a general Amber force field, J. Comput. Chem. 25 (2004) 1157–1174.

[57] R.W. Hockney, J.W. Eastwood, Computer Simulation Using Particles, Adam Hilger, 1988.

[58] J.M. Martínez, L. Martínez, Packing optimization for automated generation of complex systems' initial configurations for molecular dynamics and docking, J. Comput. Chem. 24 (2003) 819–825.

[59] L. Martinez, R. Andrade, E.G. Birgin, J.M. Martínez, PACKMOL: a package for building initial configurations for molecular dynamics simulations, J. Comput. Chem. 30 (2009) 2157–2164.

[60] W.G. Hoover, Canonical dynamics: equilibrium phase-space distributions, Phys. Rev. A 31 (1985) 1695–1697.

[61] W. Shinoda, M. Shiga, M. Mikami, Rapid estimation of elastic constants by MD simulation under constant stress, Phys. Rev. B 69 (2004) 134103.

[62] M. Brehm, M. Thomas, S. Gehrke, B. Kirchner, TRAVIS: a free analyzer for trajectories from molecular simulation, J. Chem. Phys. 152 (2020).

[63] M. Brehm, B. Kirchner, TRAVIS: a free analyzer and visualizer for Monte Carlo and molecular dynamics trajectories, J. Chem. Inf. Model. 51 (2011) 2007–2023.

[64] W. Zhao, F. Leroy, B. Heggen, S. Zahn, B. Kirchner, S. Balasubramanian, F. Müller-Plathe, Are there stable ion-pairs in room-temperature ionic liquids? MD simulations of [BMIM][PF6], J. Am. Chem. Soc. 131 (2009) 15825–15833.

[65] M. Kohagen, M. Brehm, J. Thar, W. Zhao, F. Müller-Plathe, B. Kirchner, Performance of quantum-chemically derived charges and persistence of ion cages in ionic liquids: a study of [BMIM][Br], J. Phys. Chem. B 115 (2011) 693–702.

[66] S. Spittle, I. Alfurayj, B.B. Hansen, K. Glynn, W. Brackett, R. Pandian, C. Burda, J. Sangoro, Enhanced dynamics and charge transport at the eutectic point: a new paradigm for deep eutectic solvents, JACS Au 3 (2023) 3024–3030.

[67] I.C. Yeh, G. Hummer, System-size dependence of diffusion coefficients and viscosities from MD simulations with periodic boundary conditions, J. Phys. Chem. B 108 (2004) 15873–15879.

[68] O.A. Moultos, Y. Zhang, I.N. Tsimpanogiannis, I.G. Economou, E.J. Maginn, System-size corrections for self-diffusion coefficients: CO_2, n-alkanes, PEG dimethyl ethers, J. Chem. Phys. 145 (2016).

[69] R. Yusof, E. Abdulmalek, K. Sirat, M.B.A. Rahman, Tetrabutylammonium bromide-based deep eutectic solvents and their physical properties, Molecules 19 (2014) 8011–8026.

[70] M.B.A. Rahman, K. Jumbri, M. Basri, E. Abdulmalek, K. Sirat, A.B. Salleh, Synthesis and physico-chemical properties of new tetraethylammonium-based amino acid chiral ionic liquids, Molecules 15 (2010) 2388–2397.

[71] Y. Zhang, A. Otani, E.J. Maginn, Reliable viscosity calculation from equilibrium MD simulations: a time decomposition method, J. Chem. Theory Comput. 11 (2015) 3537–3546.

[72] J.P. Cerón-Carrasco, D. Jacquemin, C. Laurence, A. Planchat, C. Reichardt, K. Sraïdi, Determination of a solvent hydrogen-bond acidity scale using solvatochromism of betaine-30 and PCM-TD-DFT, J. Phys. Chem. B 118 (2014) 4605–4614.

[73] C. Reichardt, Solvation effects in organic chemistry: a short historical overview, J. Org. Chem. 87 (2022) 1616–1629.

[74] S. Seal, K. Doblhoff-Dier, J. Meyer, Dielectric decrement for aqueous NaCl solutions: effect of ionic charge scaling, J. Phys. Chem. B 123 (2019) 9912–9921.

[75] W.M. Haynes, CRC Handbook of Chemistry and Physics, 92nd ed., CRC Press, Boca Raton, FL, 2011.

[76] S. Spittle, D. Poe, B. Doherty, C. Kolodziej, L. Heroux, M.A. Haque, H. Squire, T. Cosby, Y. Zhang, C. Fraenza, S. Bhattacharyya, M. Tyagi, J. Peng, R.A. Elgammal, T. Zawodzinski, M. Tuckerman, S. Greenbaum, B. Gurkan, M. Dadmun, E.J. Maginn, J. Sangoro, Evolution of microscopic heterogeneity and dynamics in choline chloride-based deep eutectic solvents, Nat. Commun. 13 (2022).